PNAS RESEARCH ARTICLE | CELL BIOLOGY OPEN ACCESS

The WWP1–JARID1B axis sustains acute myeloid leukemia chemoresistance

Claudia Fierro[a,1], Sara Giovannini[a,1], Valeria Moriconi[a], Claudia Fiorilli[a], Emanuele Panatta[a], Valentina Frezza[a], Federica Corigliano[a], Rosalba Pecorari[a,b], Yanan Li[a,c], Ji Zhou[a,d], Vincenza Simona Delvecchio[a], Artem Smirnov[a,b], Jose Manuel Garcia Manteiga[e], Andrea Brendolan[f], Jinping Zhang[d], Yufang Shi[c], Ivano Amelio[g], Eleonora Candi[a,b], Gerry Melino[a], and Francesca Bernassola[a,2]

Affiliations are included on p. 10.

Edited by Tak Mak, University of Toronto, Toronto, Canada; received October 19, 2024; accepted May 31, 2025

To uncover substrates mediating the oncogenic activity of WWP1 in acute myeloid leukemia (AML), we performed a proteomic analysis that identified the histone demethylase *KDM5B*/JARID1B as a candidate target. Of note, JARID1B is indispensable for efficient recruitment of several DNA damage repair factors and for damage resolution, thus negatively influencing the sensitivity of cancer cells to chemo- and radiation therapies. Validation of JARID1B as a substrate of WWP1 revealed a positive regulation of JARID1B half-life by WWP1 through the establishment of K63-linked polyubiquitin chains. As a result, downregulation of JARID1B rising from WWP1 inactivation was associated with higher H3K4me3 enrichment at JARID1B target genes in WWP1-depleted relatively to control AML cells. Integration of RNA-seq and H3K4me3 ChIP-seq data uncovered a highly significant overlap between upregulated gene expression and enriched H3K4me3 peaks after shWWP1 inactivation. We confirmed transcriptional activation of JARID1B targets in WWP1-depleted cells, supporting a role for WWP1 in regulating JARID1B activity. Coherently, upon WWP1 inactivation, we observed a defective recruitment of repair proteins after DNA damage, with subsequent reduced DNA damage repair efficiency and enhanced sensitization of AML cells to the cytotoxic activity of chemotherapeutic drugs. All together, these data identify JARID1B as a bona fide target of WWP1 and imply that WWP1-mediated regulation of JARID1B impacts its ability to modify chromatin and to recruit DNA damage repair factors, thus ultimately affecting chemosensitivity of AML cells.

protein ubiquitination | protein degradation | DNA repair | acute myeloid leukemia

Significance

To better characterize the molecular mechanism of chemoresistance in acute myeloid leukemia (AML), our study identified the histone lysine demethylase JARID1B as a substrate of the HECT E3 ubiquitin ligase WWP1. The cooperating oncogenic effect of the WWP1/JARID1B functional axis may result in chromatin remodeling events, favoring the recruitment of DNA damage repair factors, thus sustaining AML chemoresistance. Given the high rate of chemotherapy failure due to increased DNA repair in response to genotoxic drugs, our findings have potential significance for defining therapeutic strategies to overcome resistance in AML patients.

Acute myeloid leukemia (AML) is a highly heterogeneous hematological neoplasm characterized by a blockade in differentiation of hematopoietic stem cells and a clonal expansion of myeloid blasts. Even though AML is a heterogeneous disease, first-line therapeutic regimens are based on intensive chemotherapy combining cytarabine and anthracyclines. Both these agents act by causing DNA damage in leukemic blasts. Despite achieving a high rate of complete remission after therapy, the five-year overall survival is poor and especially elderly patients relapse (1). A better characterization of the molecular determinants of chemoresistance in AML may provide new biomarkers for disease risk stratification as well as novel therapeutic strategies to overcome resistance. Resistance to genotoxic drugs due to increased DNA damage repair remains one of the leading causes of chemotherapy failure and the high relapse rate in AML patients. DNA damage repair relies on DNA repair factor activation and epigenetic remodeling of chromatin spatial structure, which in turn facilitates the recruitment of the repair factors (2, 3). In particular, DNA double-strand breaks (DSBs), the most lethal DNA aberrations produced by genotoxic agents, can be repaired by two major mechanisms: the nonhomologous end-joining (NHEJ) and the homologous recombination (HR) repair systems (4).

The HECT-type E3 ubiquitin ligase WWP1 is an oncogenic protein, overexpressed in several cancers including AML, in which it exerts its protumorigenic activity through multiple mechanisms, including promoting cancer cell cycle progression and survival (5). WWP1 depletion arrests the cell cycle at the G1 phase through the ubiquitin-mediated proteasomal degradation of *CDKN1B*_p27 and cytoplasmic p53 translocation (6, 7). In addition, we have recently shown that WWP1 inactivation increases the basal levels of cellular DNA damage in AML cells by supporting TXNIP-dependent accumulation of reactive oxygen species (ROS) (8). Hence, we have proposed that WWP1 overexpression in AML blasts would favor leukemic cell survival by limiting ROS generation, therefore sustaining cancer cell fitness.

Author contributions: F.B. designed research; C. Fierro, S.G., V.M., C. Fiorilli, E.P., V.F., F.C., R.P., Y.L., J. Zhou, V.S.D., and A.S. performed research; C. Fierro, S.G., V.M., C. Fiorilli, E.P., F.C., R.P., Y.L., J. Zhou, V.S.D., A.S., J.M.G.M., A.B., J. Zhang, Y.S., I.A., E.C., G.M., and F.B. analyzed data; and S.G. and F.B. wrote the paper.

The authors declare no competing interest.

This article is a PNAS Direct Submission.

[1]C.F. and S.G. contributed equally to this work.

[2]To whom correspondence may be addressed. Email: bernasso@uniroma2.it.

This article contains supporting information online at https://www.pnas.org/lookup/suppl/doi:10.1073/pnas.2421159122/-/DCSupplemental.

Published July 8, 2025.

The *KDM5* family of epigenetic modulators includes four Jumonji (JmjC) domain-containing paralogs, *KDM5A* (JARID1A), *KDM5B* (JARID1B), *KDM5C* (JARID1C), and *KDM5D* (JARID1D). JARID proteins are histone lysine demethylases, highly specific toward di- and trimethylated states of Lys4 of histone H3 (H3K4me2 and H3K4me3), which are marks of active transcription, frequently found in the promoter region of transcribed genes (9). Therefore, as erasers of the transcriptional activating mark H3K4me3 at gene promoter regions, they act as epigenetic repressors. Furthermore, JARID proteins can be recruited to intragenic H3K36me3 sites within actively transcribed genes to safeguard transcriptional elongation by repressing unwanted intragenic transcription (10).

JARID1B is amplified or overexpressed in several cancers, and elevated expression levels of JARID1B are associated with decreased survival and drug resistance (11–14). Scalea and collaborators reported that JARID1B expression is increased in AML patients relative to normal mature $CD34^+$ cells (15). On the other hand, tumor-suppressing roles for JARID1B have been reported in specific molecular subsets of AML, such as NUP98-$NSD1^+$ and MLL-rearranged AML (16, 17).

Similarly to WWP1 silencing, inhibition of JARID1B results in reduced viability and cell cycle arrest of leukemia cells (18, 19). JARID1B positively regulates cell cycle progression by epigenetically repressing the transcription of cell cycle checkpoint genes including *CDKN1A*_p21 (20) and *CDKN1B*_p27 (21). Furthermore, it is well established that the demethylase activity of JARID1B is necessary for efficient recruitment of several DNA damage repair factors including NHEJ (Tumor suppressor p53-binding protein 1 [53BP1], Ku autoantigen 70 kDa subunit, Ku autoantigen 80 kDa subunit, DNA-dependent protein kinase catalytic subunit [DNA-PKcs]), HR (Breast cancer type 1 susceptibility protein [BRCA1]), and DNA single-strand break repair (X-ray repair cross-complementing protein 1 [XRCC1]) components to damaged DNA (22–24). As a result, JARID1B facilitates resolution of DNA damage and promotes resistance to chemo- and radiation therapy. Coherently, genetic or pharmacological inhibition of JARID1B leads to specific accumulation of H3K4me3 at sites marked by γH2AX deposition, prevents recruitment of DNA repair factors, and favors accumulation of DNA damage (22–24). Overall, current evidence points toward JARID1B as a tumor-promoting gene.

Here, we combine a mass spectrometry-based screening, ChIP and RNAseq analyses to unveil the role of WWP1 on JARID1B-regulated histone modifications and gene expression alterations associated with DNA repair and drug resistance.

Results

JARID1B Acts as a Substrate for WWP1-Mediated Polyubiquitination. To identify WWP1 targets underlying its oncogenic activities in leukemia, we have conducted ubiquitination proteomics in control versus WWP1-depleted NB4 human promyelocytic leukemia cells (*SI Appendix*, Fig. S1*A*). This affinity capture-based methodology allows the quantitative analysis of enriched ubiquitinated peptides and ubiquitination site identification (UbiScan® Cell Signaling Technology) (24, 25). We have identified 110 putative targets (hits with negative fold change in WWP1-depleted cells) of WWP1 (Fig. 1 *A* and *B* and *SI Appendix*, Fig. S1*B* and Dataset S1). Among the transcriptional regulators potentially modified by WWP1, we uncovered the histone lysine demethylases *KDM5B*/JARID1B (Fig. 1 *A* and *B*), whose catalytic activity is required to induce efficient repair of DSBs (22). Coimmunoprecipitation assays confirmed the occurrence of protein–protein interactions between WWP1 and JARID1B (Fig. 1 *C–E* and *SI Appendix*, Fig. S1*C*). The association between WWP1 and JARID1B was also confirmed using purified recombinant proteins in in vitro pulldown assays, hence implying specific and direct binding of the E3 to its substrate (Fig. 1*F*). The interaction of HECT E3s with their substrates is mediated by WW domains, which usually recognize proline-rich motifs such as PPxY, PPLP, PXY, and phosphorylated serine/threonine-proline sites (6, 7). To map the domains mediating the WWP1–JARID1B interaction, we mutagenized five proline-rich motifs in JARID1B, including three canonical PXY motifs and two SP phosphorylation sites commonly recognized by HECT-type E3s. We also generated WWP1 mutants lacking individual WW domains (1 to 4). Coimmunoprecipitation experiments with WWP1 and JARID1B mutants revealed that the WWP1–JARID1B interaction is mediated by the PAY motif of JARID1B (Fig. 1*G* and *SI Appendix*, Fig. S1 *D–I*). However, mutation of the PAY motif was not sufficient to completely disrupt the interaction, suggesting that an additional, noncanonical domain, may also contribute to their binding. Reciprocal coimmunoprecipitations between JARID1B and WWP1 mutants lacking individual WW domains revealed that none of the deletions was sufficient to abolish the interaction with JARID1B (*SI Appendix*, Fig. S1 *J–L*). These findings suggest that either the retention of any of the other three functional WW domains is sufficient to compensate for the loss of a single WW domain, or that specific combinations of WW domains are required for the interaction with JARID1B. Notably, similar WW domain redundancy has been described for the HECT-type E3 NEDD4L, supporting the concept of cooperative or compensatory interactions among WW domains (26).

WWP1 shows preferential selectivity for Lys11 (K11), Lys27 (K27), Lys48 (K48), and Lys63 (K63) polyubiquitin linkage synthesis on its protein targets (27–29). To further investigate the ability of WWP1 to modify JARID1B, we performed in vivo ubiquitination assays in cells expressing either wild-type WWP1 or a catalytically inactive mutant (C890A), in the presence of wild-type ubiquitin or the K63R (Lys63 to Arg, which abolishes its ability to elongate polyubiquitin chains on protein substrates) and the K63-only (where all Lys residues except K63 are mutated) ubiquitin mutants. Additionally, we generated a JARID1B mutant (Lys 153 to Ala) lacking the Lys identified by the UbiScan proteomics approach as a potential WWP1 ubiquitination site. Using K63 linkage-specific polyubiquitin antibodies, we demonstrated that WWP1 catalyzes K63-polyubiquitination of JARID1B at Lys153, in a manner dependent on its catalytic activity (Fig. 2*A* and *SI Appendix*, Fig. S1*J*). Of note, we also found that JARID1B polyubiquitination is reduced upon inactivation of WWP1 in NB4 cells (Fig. 2*B*).

To confirm that WWP1 directly recruits and modifies JARID1B and to validate the type of ubiquitin linkages implicated in WWP1-mediated JARID1B modification, we exploited other ubiquitin mutants in in vitro reconstituted ubiquitination assays. Consistent with WWP1 directly binding JARID1B, we found that WWP1 is able to ubiquitinate JARID1B under in vitro conditions (Fig. 2*C*). Moreover, JARID1B ubiquitination was prevented only in the presence of the K63R ubiquitin mutant, proving that WWP1 promotes polyubiquitination of JARID1B via K63 of ubiquitin (Fig. 2*C*).

WWP1 Increases JARID1B Protein Half-Life. We then examined the effects of polyubiquitination of JARID1B by WWP1. WWP1 silencing in the NB4 cell line led to a reduction of JARID1B cellular and nuclear abundance (Fig. 3 *A* and *B*). In contrast, WWP1 silencing did not affect *KDM5B* mRNA levels (Fig. 3*C*), suggesting posttranslational regulation of JARID1B by WWP1. The other JmjC enzymes were differentially expressed in NB4 cells, but their mRNA and protein levels were always lower than that of *KDM5B* (Fig. 2 *D* and *E*), with the *KDM5D* transcript

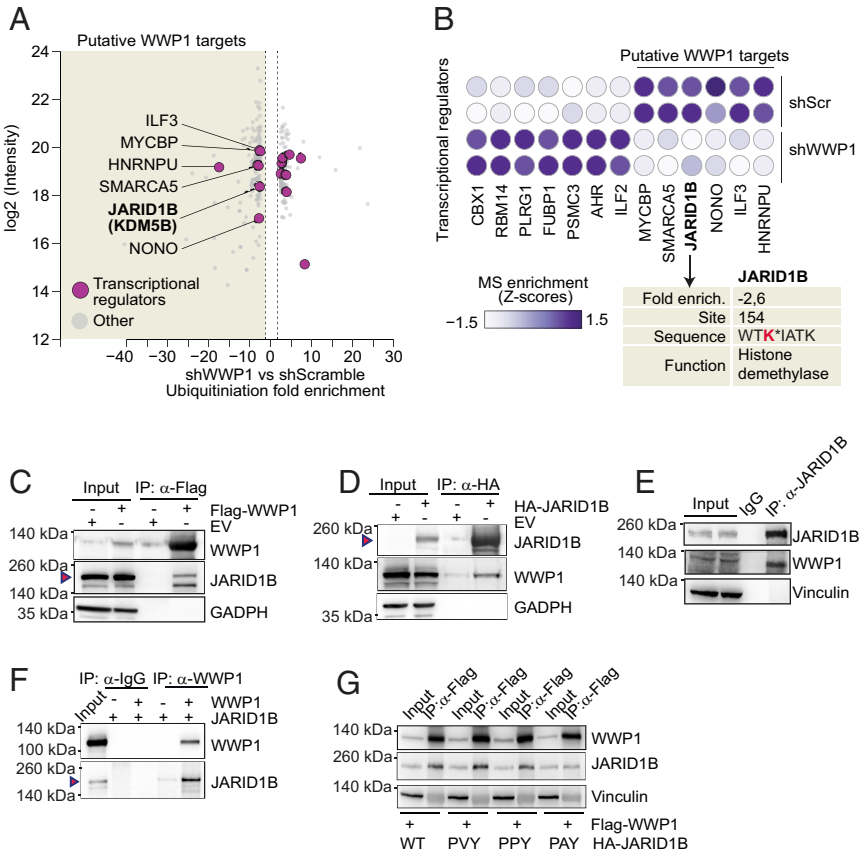

Fig. 1. Identification of JARID1B as a WWP1 substrate. (*A* and *B*) Proteomic analysis (UbiScan® Cell Signaling Technology) identifies JARID1B as a candidate substrate of WWP1. (*A*) Volcano plot showing intensity and enrichment of ubiquitinated peptides in shWWP1 versus control sample. Beige shading highlights putative WWP1 targets. Transcriptional regulators are shown in magenta. (*B*) Heatmap showing Z-scores of intensities of identified peptides belonging to transcriptional regulator set of proteins. (*C* and *D*) Representative western blots for the coimmunoprecipitation assays. HEK293T cells were transfected with Flag-WWP1 (*C*) or HA-JARID1B (*D*). Cellular extracts were pulled down with anti-Flag (*C*) and anti-HA (*D*) antibodies and then analyzed by western blot with anti-JARID1B and anti-WWP1 antibody, respectively. GADPH was used as loading control. Three independent experiments were carried out. (*E*) Representative western blot showing binding of endogenous JARID1B and WWP1 in NB4 cells. Cellular lysates were immunoprecipitated with anti-JARID1B or an IgG isotype control antibody and then subjected to western blot with anti-WWP1 and anti-JARID1B antibodies. Vinculin was used as loading control. Three independent experiments were carried out. (*F*) Representative western blots of the in vitro pull-down experiments. Purified recombinant WWP1 and JARID1B proteins were incubated overnight at 4 C. WWP1 was then immunoprecipitated by using anti-WWP1 antibody conjugated with protein A beads and the immunocomplexes were subjected to western blot with anti-JARID1B antibody. Isotypic IgG conjugated with Protein A beads were used as a negative control. Three independent experiments were carried out. (*G*) Representative western blots of coimmunoprecipitation assays from HEK293T cells cotransfected with Flag-WWP1 and either wild-type or the three PXY mutants of HA-JARID1B. Total cellular extracts were immunoprecipitated with anti-Flag antibody and subsequently analyzed by western blot with anti-HA antibody. Three independent experiments were carried out.

being undetectable in this cell line (Fig. 3*D*). In addition, WWP1 inactivation did not influence JARID1A, JARID1C, and JARID1D protein levels (Fig. 3*E*), confirming the specificity of the WWP1-regulatory mechanism for JARID1B. We excluded the possibility that WWP1 regulates lysine demethylase 2B (KDM2B), another histone lysine demethylase targeting H3K4me3 (30), as KDM2B protein levels were unaffected in WWP1-depleted NB4 cells compared to controls (Fig. 3*E*). We next examined the turnover rate of JARID1B protein using a cycloheximide (CHX) chase assay and found that WWP1 overexpression significantly increased JARID1B half-life compared to control cells (Fig. 3*F*).

These results demonstrate that JARID1B protein stability is positively regulated by WWP1-mediated K63-linked ubiquitin chain synthesis. While K48- and K11-linked polyubiquitin chains primarily mark proteins for proteasomal degradation, the K63-linked chains usually do not serve as proteasome-targeting signals, but rather contribute to a range of proteolytic-independent cellular functions, including protein stabilization (31, 32).

WWP1 Regulates the Histone Demethylase Activity of JARID1B. Downregulation of JARID1B in WWP1-depleted AML cells was coherently associated with increased global levels of H3K4me3 (Fig. 4*A* and *SI Appendix*, Fig. S2*A*), suggesting a role for WWP1 in modulating the histone demethylase activity of JARID1B. To further explore the effect of WWP1 silencing on JARID1B function, we performed ChIP sequencing (ChIP-seq) for H3K4me3 in control and WWP1-silenced NB4 cells. ChIP-Seq data revealed increased H3K4me3 enrichment at promoter regions in WWP1 knockdown compared to control AML cells (Fig. 4*B* and *SI Appendix*, Fig. S2*B*), which is in line with the ability of JARID1B to influence H3K4 methylation patterns at transcription start sites (TSSs) (33). Following WWP1 depletion, only a minority of the H3K4me3 enriched ChIP-seq peaks showed a reduction (approximately 20%) whereas the remaining peaks increased relatively to control cells (*SI Appendix*, Fig. S2*C*). Furthermore, downregulated H3K4me3 peaks are not enriched at the TSS (*SI Appendix*, Fig. S2*C*) and have a lower Maxtag score as compared to the upregulated ones (*SI Appendix*, Fig. S2*D*). Remarkably, inactivation of WWP1 resulted in increased H3K4me3 enrichment at JARID1B target genes (Fig. 4 *C*–*E* and Dataset S2) as well as at the 200 most enriched genomic regions for H3K4me3 (*SI Appendix*, Fig. S2 *E*-*G* and Dataset S3). Since WWP1 inactivation has no effect on protein levels of the other *KDM5* paralogs or KDM2B (Fig. 3*E*), changes in H3K4me3 levels

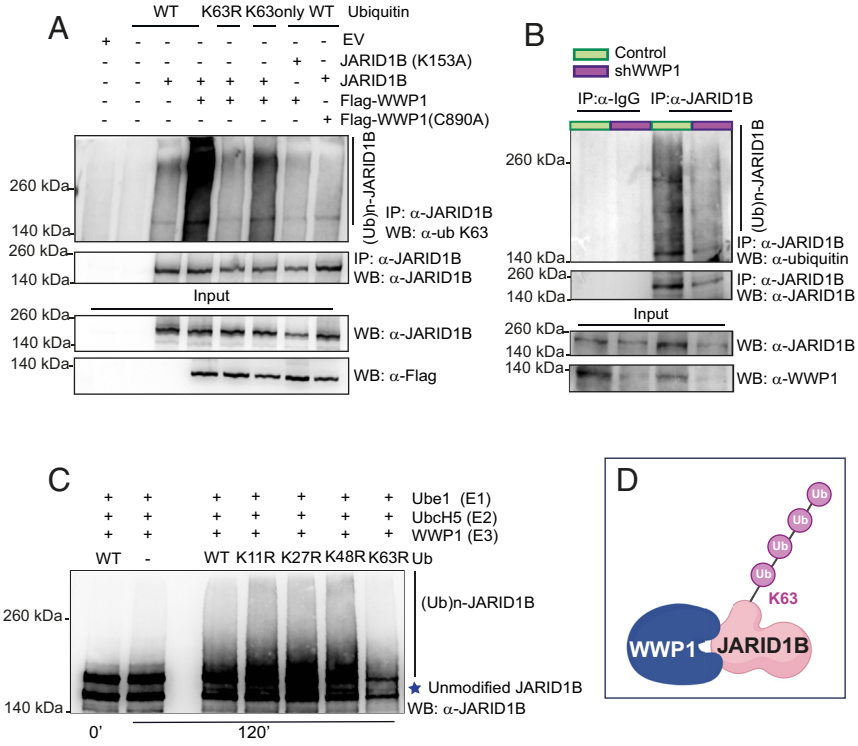

Fig. 2. WWP1 modifies JARID1B via Lys63 polyubiquitin linkages. (*A*) Representative western blot analysis of the in vivo ubiquitination of JARID1B by WWP1. HEK293T cells were cotransfected with the indicated plasmids. Ubiquitinated JARID1B was assessed by immunoprecipitation with anti-JARID1B antibody, followed by western blot with a K63-linkage specific polyubiquitin antibody. Three independent experiments were carried out. (*B*) Ubiquitinated JARID1B was assessed in control and WWP1-depleted NB4 cells following immunoprecipitation of cellular extracts with anti-JARID1B or an IgG isotype control antibody. Immunoprecipitates were then subjected to western blot with anti-ubiquitin antibody (*C*) Representative in vitro ubiquitination assay. Purified recombinant JARID1B and WWP1 proteins were incubated in the presence of E1 (Ube1), E2 (UbcH5), and either wild-type ubiquitin or Ub K-R ubiquitin mutants for 2 h at 30 °C. Negative controls were included: time 0 reaction (lane 1) and reaction carried out for 2 h in the absence of ubiquitin (lane 2). In vitro ubiquitination reactions were then subjected to SDS-PAGE and immunoblotted with JARID1B antibody. (*D*) Schematic representation of JARID1B modification by WWP1 through the generation of K63-linked ubiquitin chains.

in WWP1-depleted leukemia cells are expected to primarily result from JARID1B regulation. To further dissect WWP1-mediated regulation of JARID1B, we carried out transcriptomic profiling of NB4 cells following WWP1 silencing. Replicated RNA-seq profiles within the same sample group were highly consistent with a total of 1.032 differentially expressed genes (DEGs) (576 up-regulated and 461 down-regulated genes) in WWP1-depleted relatively to control cells (*SI Appendix*, Fig. S2 *H* and *I*). Integration of RNA-seq and H3K4me3 ChIP-seq data uncovered a highly significant overlap between upregulated gene expression and enriched H3K4me3 peaks after shWWP1 (O.R. 12.2, Fisher *P*-value 2.65×10^{-30}) (Fig. 3*F* and Dataset S4). We also retrieved *KDM5B* ChIP-seq data from public datasets (K562 leukemic cells, GSM1003586), to perform an integration analysis of the *KDM5B* bound genomic regions, with the H3K4me3 ChIP-seq and RNA-seq data obtained following WWP1 silencing in NB4 cells. By overlapping these data, we found that among the upregulated genes in shWWP1 cells, 58 genes have a peak of JARID1B near the TSS in K562 cells and 6 of them display also a peak in H3K4me3 after shWWP1 silencing in NB4 cells (Fig. 4*F*). Expression analysis of JARID1B targets confirmed a significant increase in their transcript levels in WWP1-depleted cells, including those genes that emerged from the integrated analysis (Fig. 4 *F* and *G*). Among these, the *CDKN1A* (p21) gene was the most upregulated (Fig. 4*G* and *SI Appendix*, Fig. S2*J*), indicating a cooperative action of WWP1 and JARID1B in promoting cell cycle arrest. The expression of selected genes (among the 200 most enriched genomic regions), showing H3K4me3 enrichment after shWWP1 silencing (*SI Appendix*, Fig. S2*F*), was also upregulated in shWWP1 relatively to control AML cells (*SI Appendix*, Fig. S2*K*).

Importantly, we observed a similar trend when looking at genes differentially expressed in *WWP1* low versus *WWP1* high expressing AML tumors from TCGA (Fig. 4*H*). Fifteen genes, enriched in *WWP1* low expressing leukemias, were JARID1B targets, including *CDKN1A*, whose expression was negatively correlated with *WWP1* expression in TCGA AML patients (Fig. 4*I*). We further confirmed these data by profiling healthy donor samples and AML specimens with low or high WWP1 expression by RT-qPCR. Coherently with the previous findings, we observed a significant decrease in *CDKN1A* mRNA levels in tumors with high versus low *WWP1* levels or with healthy biopsies (Fig. 4*J*).

JARID1B is known to affect the H3K4me3-dependent recruitment of repair factors in response to DNA damage, by modifying the chromatin landscape instead of transcriptionally regulating the DDR (22–24). Coherently, the RNA-Seq data did not reveal any statistically significant difference in the expression of genes related to the DDR upon WWP1 silencing in NB4 cells, with the only exception of the nucleotide excision repair pathway (Dataset S5 *A* and *B*). All together, these data support a role for WWP1 in regulating JARID1B activity.

WWP1-Depleted Cells Show an Impairment in the Formation of DNA-Damage Response (DDR) Foci. We next sought to test the hypothesis that reduced JARID1B histone demethylase activity and subsequent H3K4me3 enrichment in WWP1-depleted AML cells would lead to a defective recruitment of repair proteins following DNA damage. We assessed the phosphorylated form of histone variant H2AX (γH2AX), an indicator of DSBs, following administration of the radiomimetic chemotherapeutic agent bleomycin (BLM), that induces single and double-strand DNA

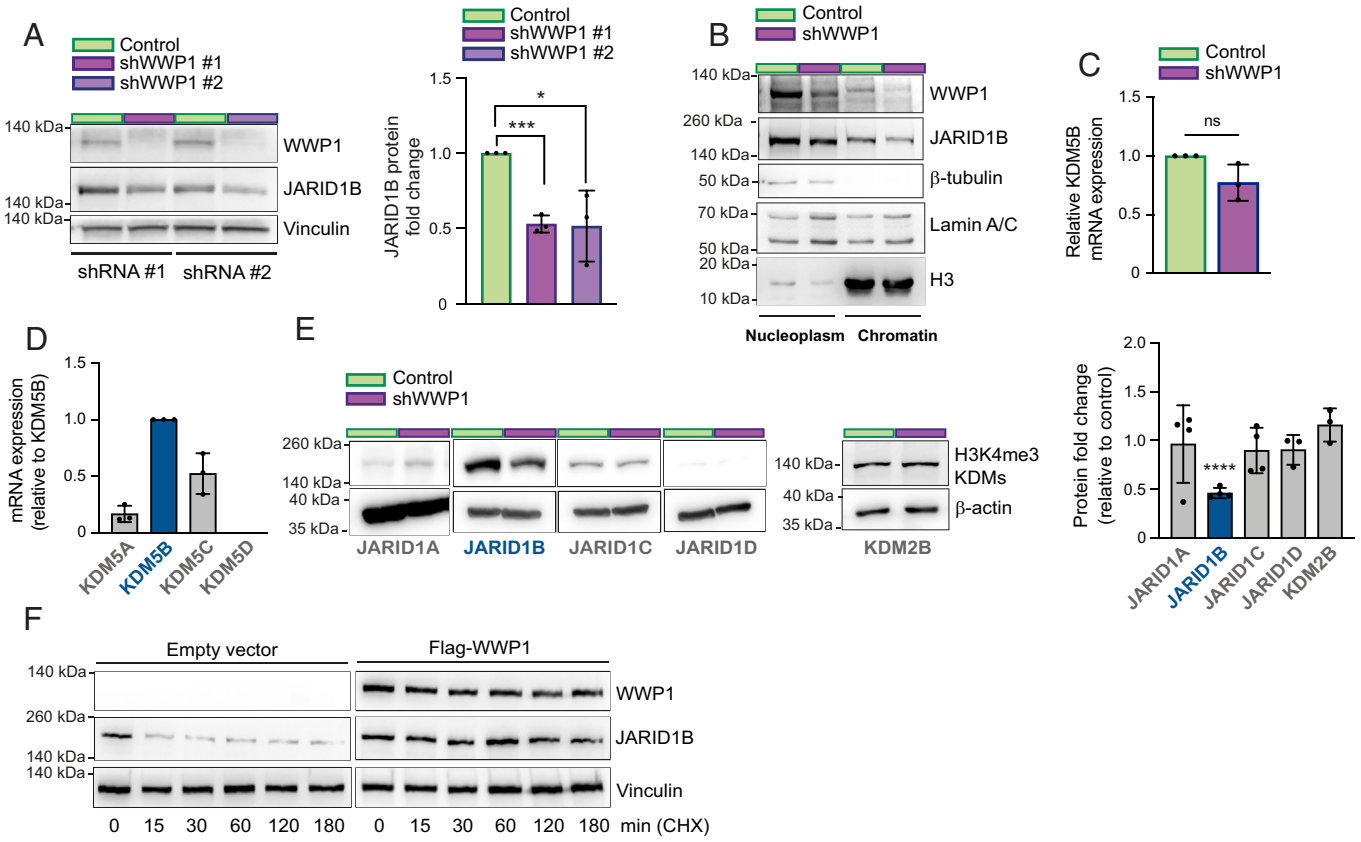

Fig. 3. WWP1 silencing leads to JARID1B protein destabilization. (*A*) Representative western blot analysis of JARID1B protein levels in control and WWP1-depleted NB4 cells (*Left* panel). Two different clones of NB4/Tet-On/shWWP1 cells were analyzed. Three independent experiments were carried out. Fold changes were quantified using ImageJ software (*Right* panel). (*B*) Representative western blot analysis of JARID1B protein levels in chromatin-free soluble and in chromatin fractions extracted from control and WWP1-depleted NB4. (*C*) mRNA levels of *KDM5B* in control and shWWP1-depleted NB4 cells were analyzed by RT-qPCR. Relative abundances of transcripts were quantified and normalized to *TBP*. Values represent the mean ± SD from three independent experiments. (*D*) Detection of *KDM5A*, *KDM5B*, *KDM5C*, and *KDM5D* transcript levels by RT-qPCR. Relative abundances of mRNAs were normalized to *TBP*. Values represent the mean ± SD from three independent experiments. (*E*) Representative western blot analysis of JARID1A, JARID1B, JARID1C, JARID1D, and KDM2B protein levels following WWP1 silencing in NB4 cells (*Left* panels). Protein level fold changes were quantified using ImageJ software and normalized to β-actin expression (*Right* panel). Statistically significant differences were calculated by Student's *t* test. (*F*) Representative western blot analysis of WWP1 and JARID1B protein levels in control and WWP1 overexpressing HEK293T cells after protein synthesis blockade with CHX (50 μg/ml). Vinculin was used as loading control. Statistically significant differences were calculated by Student's *t* test. **P* < 0.05, ****P* < 0.001, *****P* < 0.0001.

breaks, and found a significant decrease in the number of γH2AX decorated foci in WWP1-depleted relatively to control cells (Fig. 5 *A–D* and *H* and *SI Appendix*, Fig. S3 *A–D*). γH2AX then serves as a docking site to tether several DDR proteins to the damaged site, including components of both NHEJ and HR repair systems (34). DDR factors are recruited to nuclear foci where they colocalize and interact with γH2AX. Indeed, accumulation of the checkpoint NHEJ-related repair factor 53BP1 at DNA breaks is mediated by its binding to γH2AX (35, 36). We observed that WWP1-silenced NB4 cells manifested impaired 53BP1 foci formation upon BLM administration (Fig. 5 *A*, *E*, and *I* and *SI Appendix*, Fig. S3*A*). Similarly, the assembly of phosphorylated DNA-PK foci at DNA strand breaks, a critical initial step for NHEJ repair (37), was significantly diminished following WWP1 silencing (Fig. 5 *B*, *F*, and *J* and *SI Appendix*, Fig. S3*B*). We also monitored the formation of BRCA1 foci upon BLM exposure and found a similar impairment in BRCA1 recruitment in WWP1-depleted leukemia cells (Fig. 5 *C*, *G*, and *K* and *SI Appendix*, Fig. S3*C*), implying also a reduction in HR activation. As shown in *SI Appendix*, Fig. S3 *E–G*, the percentages of cells showing DDR-positive foci were significantly lower in WWP1-depleted cells.

The pan JmjC inhibitor JIB-04, which increases H3K4me3, has been shown to delay DDR foci resolution after radiation exposure and to enhance the response of cancer cells to DNA damage (22). Of note, the Authors have demonstrated that knockdown of *KDM5B*, but not silencing of the other JmjC enzymes, is capable to phenocopy the effect of JIB-04 on DNA repair, excluding the requirement for the other paralogs in recruiting DDR proteins on DNA lesions. We next determined the effect of JIB-04 on leukemia cells following administration of BLM and found that similarly to WWP1 silencing-dependent JARID1B inactivation, pharmacological inhibition of JARID1B weakened the formation of DDR foci in response to DNA damage (*SI Appendix*, Fig. S4).

Overall, these findings suggest that alterations in DDR factor recruitment elicited by WWP1 inactivation may impair the efficiency of DNA repair played through either NHEJ or HR signaling pathways. These data also imply that, similarly to JARID1B inhibition (*SI Appendix*, Fig. S4), the DDR defects observed in the absence of WWP1 (Fig. 5 and *SI Appendix*, Fig. S3) cannot be ascribed to a specific repair system for damaged DNA, but rather to a common chromatin state that is dependent on the availability of H3K4me3.

DNA Damage Resolution Is Delayed in WWP1-Depleted Cells. To further explore the outcome of WWP1-mediated regulation of DDR protein recruitment in response to DNA damage, we next evaluated whether WWP1 depletion affects the efficiency of the DNA repair process. To this aim, we evaluated the repair of BLM-induced DNA strand breaks by performing comet assays. The level

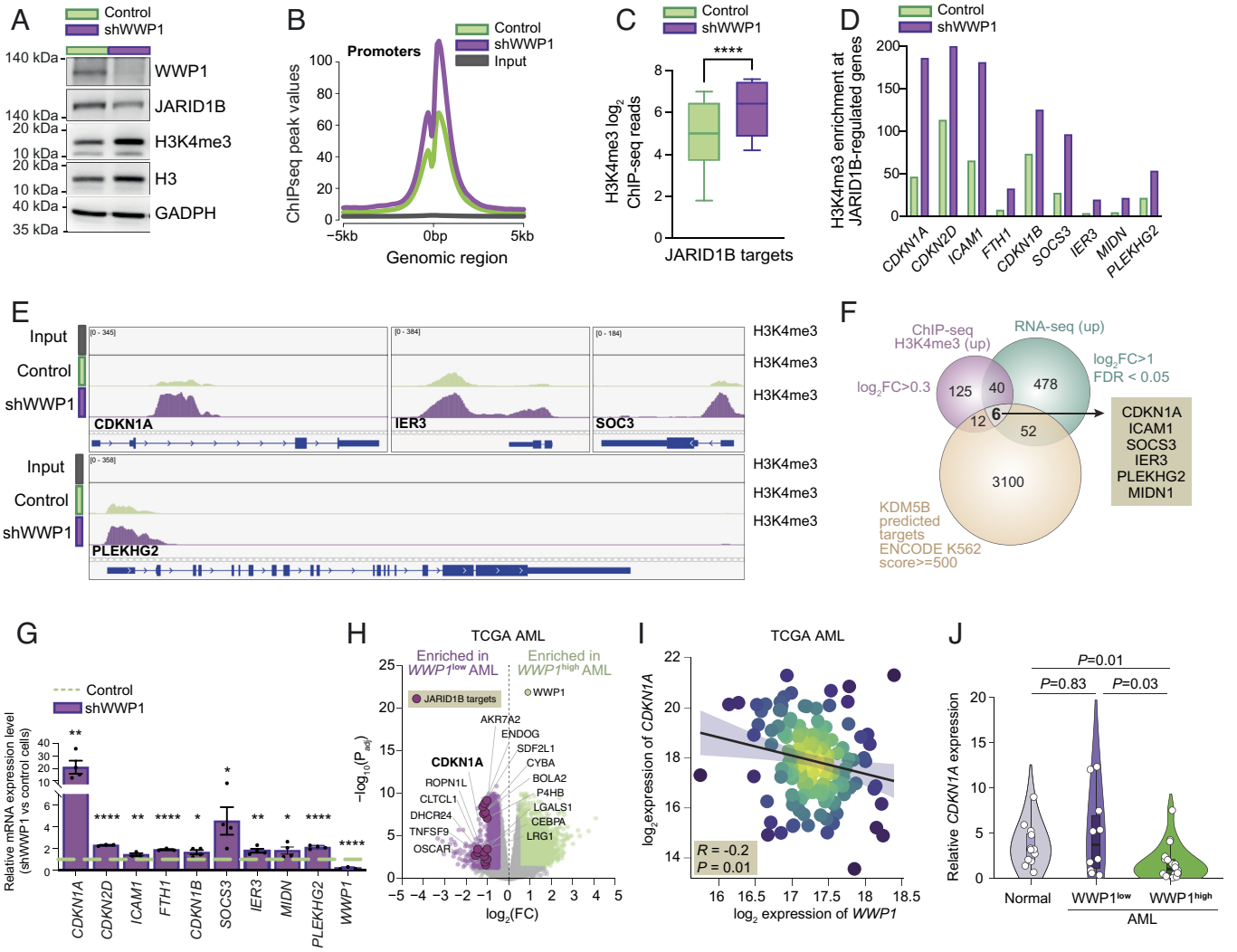

Fig. 4. WWP1 regulates the histone demethylase activity of JARID1B. (*A*) Representative western blot analysis of H3K4me3 protein levels following WWP1 silencing in NB4 cells. Three independent experiments were carried out. (*B*) Distribution of the H3K4me3 signal around genome-wide promoters as assessed by ChIP-sequencing in WWP1-depleted relatively to control AML cells. (*C*) Box plots showing general H3K4me3 enrichment at JARID1B target genes in control and WWP1-knockout NB4 cells (Dataset S2). Y-axis units represent log2 H3K4me3 average coverage values in control and shWWP1 NB4 cells. (*D*) H3K4me3 enrichment at JARID1B selected target genes after WWP1 silencing in NB4 cells. Y-axis units represent log2 H3K4me3 coverage average values. (*E*) Genomic snapshots of plotted ChIP-seq tracks of H3K4me3 across the indicated JARID1B target genes. (*F*) Venn diagram showing overlap of upregulated DEGs in shWWP1 NB4 cells (log2FC > 1 and FDR < 0.05), increased H4K4me3 enrichment after WWP1 inactivation (shrunken log2FC > 0.3), and the genome-wide occupancy of JARID1B in K562 leukemia cells (*KDM5B* predicted targets from ChIP-seq data in K562 cells). The box indicates JARID1B target genes in common among the three datasets. (*G*) Real-time RT-PCR analysis of selected JARID1B-regulated genes following WWP1 gene silencing in NB4 cells. Relative abundances of mRNAs were normalized to *TBP* and expressed as fold changes of shWWP1 cells relative to controls (dotted green line). Values represent the mean ± SD from three or four independent experiments (*H*) Volcano plot of genes differentially expressed in *WWP1* low versus *WWP1* high expressing AML patients from TCGA. Significantly enriched genes are shown in magenta (enriched in *WWP1* low expressing samples) or green (enriched in *WWP1* high expressing samples). Padj < 0.05 and abs(log2FC) > 1 were used as thresholds. (*I*) Dot plot showing correlations between *CDKN1A* and *WWP1* log2 expression levels in TCGA AML samples. Samples are colored by density of neighbors using ggpointdensity algorithm. Pearson correlation R and *P* value are shown. (*J*) Real-time RT-PCR analysis of *CDKN1A* expression in human peripheral blood mononuclear cells from healthy donors (n = 12), *WWP1* low (n = 10), or *WWP1* high (n = 20) AML samples. Relative abundances of mRNAs were normalized to *TBP* and expressed as relative values. Values are shown as violin plots. *P* value by the Kruskal–Wallis test. The Y-axis represents log2RPKM values. **P* < 0.05, ***P* < 0.01, *****P* < 0.0001.

of DNA damage was monitored at different time points following BLM treatment. Depletion of WWP1 increased the number of basal and BLM-induced DNA strand breaks relatively to control cells (Fig. 6 *A* and *B*). We also observed a significant delay in the clearance of BLM-induced DNA strand breaks in WWP1 knockdown cells, with a decline in the percentage of tail DNA in control cells being already statistically significant 3 h after DNA damage occurrence (Fig. 6 *A* and *B*). To further understand the DSB repair defect caused by WWP1 inactivation, we measured the efficiency of repair by NHEJ and HR, the two main pathways of cellular DNA DSB repair by employing established plasmid-based reporter systems (38). U2OS EJ-DR cells contain stable copies of both NHEJ and HR repair assays (Fig. 6*C*). Of note, both NHEJ and HR repair mechanisms were significantly inhibited in WWP1-depleted U2OS EJ-DRs cells (Fig. 6 *D* and *E* and *SI Appendix*, Fig. S5 *A–C*). To rule out the possibility that the observed impairment in HR repair activity (Fig. 5*E*) may result from G0/G1 arrest induced by WWP1 inactivation, we measured the cell cycle profile of WWP1-depleted U2OS EJ-DRs. However, we did not observe differences in the cell cycle profile of U2OS EJ-DRs cells following silencing of WWP1 as compared to control cells (*SI Appendix*, Fig. S5*D*).

WWP1 Inactivation Sensitizes AML Cells to the Cytotoxic Activity of DNA-Damaging Chemotherapeutic Drugs. Based on these findings, we reasoned that WWP1-depleted leukemic

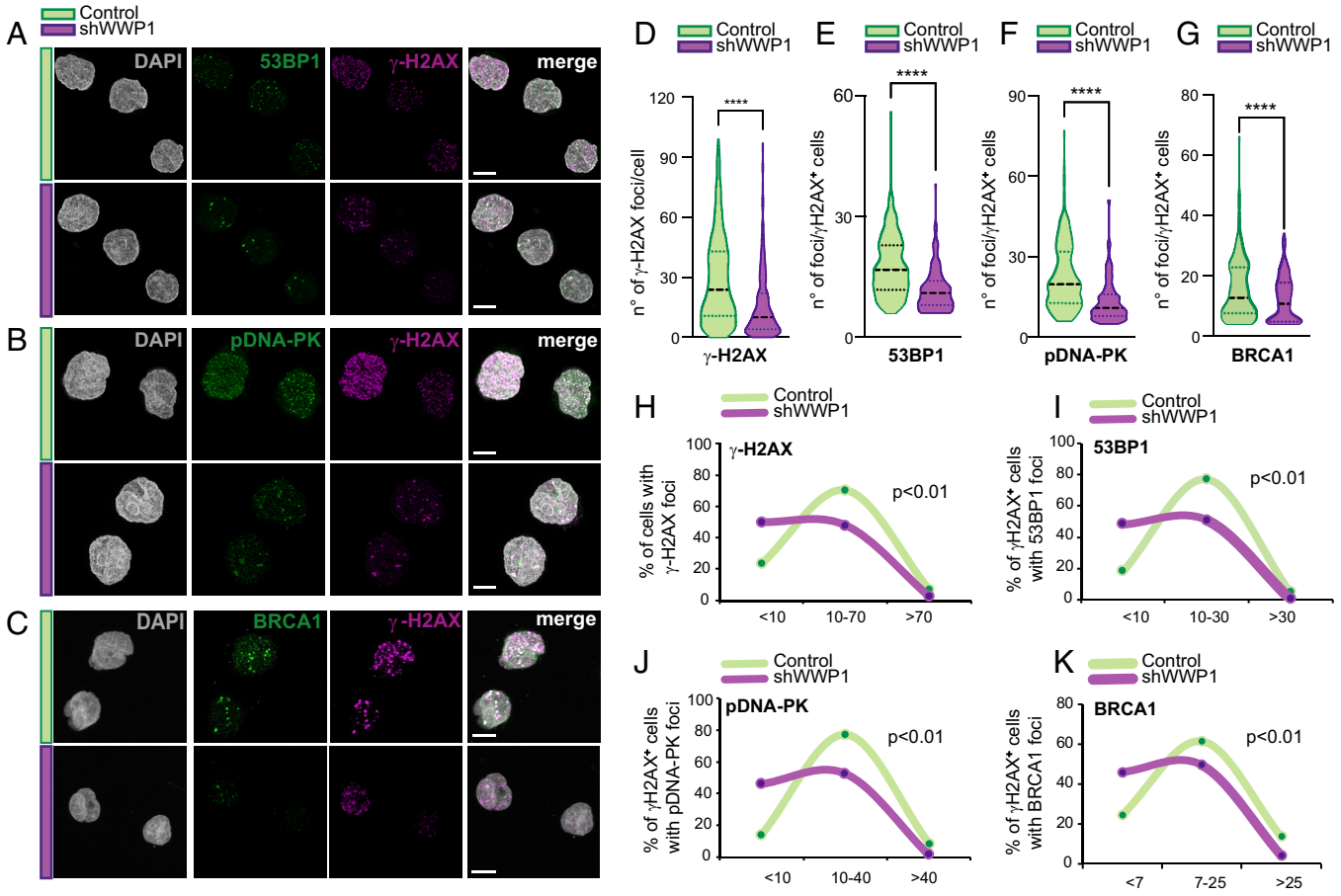

Fig. 5. WWP1 inactivation impairs the assembly of DDR foci in response to DNA damage. (*A–C*) Representative confocal images of DDR foci detected in BLM (40 μg/ml) treated control and WWP1-depleted AML cells. DNA damage foci have been detected following double immunostaining for γH2AX (purple) and one of the following repair proteins: 53BP1 (green, panel *A*), pDNA-PKcs (green, panel *B*), and BRCA1 (green, panel *C*). (Scale bar, 10 μm.) (*D–G*) Quantification of the number of γH2AX, 53BP1, pDNA-PKcs, and BRCA1 positive foci/cell. 53BP1, pDNA-PKcs, and BRCA1 foci evaluation has been performed in γH2AX positive cells (around 300 nuclei per condition); data are shown as median with quartiles and analyzed using the two-tailed unpaired *t* test. ****$P < 0.0001$. (*H–K*) Representation of cell population as percentage of cells with the indicated number of DNA damage foci (X-axis); data on shWWP1 condition (purple line) are shown as deviation from the Gaussian distribution set for the control sample (green line); *P* value has been calculated using the chi-square (X^2) test with 2 degrees of freedom. Immunofluorescence staining has been repeated three times independently.

cells might be more sensitive to DNA-damaging drugs. We therefore evaluated the interaction between WWP1 silencing and chemotherapy exposure. We selected drugs for their ability to directly or indirectly induce DNA damage. Anthracyclines (doxorubicin/daunorubicin) and cytarabine (Ara-C) are the main mainstay chemotherapeutic drugs for AML (39). A combination of Ara-C, mitoxantrone, and etoposide is instead commonly employed as second-line therapy for relapsed/refractory AMLs. Anthracyclines and etoposide are topoisomerase II poisons that induce DNA DSBs. AraC determines stalling replication forks and, as a result, it generates DNA DSBs. We also used BLM to efficiently induce DNA DSBs. WWP1-depleted NB4 cells were treated with the following drugs: AraC (Fig. 7*A*), doxorubicin (Fig. 7*B*), etoposide (Fig. 7*C*), and BLM (*SI Appendix*, Fig. S6). A significant synergism between WWP1 depletion and drug administration in reducing the growth potential of AML cells was observed for all the drugs tested three days after treatment (Fig. 7 *A–C* and *SI Appendix*, Fig. S6*A*). The ability of WWP1 inhibition to increase the cytotoxicity of chemotherapy was confirmed by detection of apoptotic markers. The combination of WWP1 silencing and chemotherapy significantly increased annexin-V positivity (Fig. 7*D* and *SI Appendix*, Fig. S6*B*), as well as caspase 3 and PARP cleavage (Fig. 7 *E–G* and *SI Appendix*, Fig. S6 *C–E*), relatively to each individual condition. Overall, these findings demonstrate that upon WWP1 depletion, AML blasts become more sensitive to genotoxic insults.

Discussion

In this study, we provide insights into the molecular events that lead to increased chemosensitivity of AML cells after silencing of the E3 WWP1. We have uncovered the histone demethylase JARID1B as a substrate for the E3 ubiquitin ligase activity of WWP1. WWP1-mediated K63-linked polyubiquitination of JARID1B positively affects its protein stability. Proteins tagged with K63-polyubiquitin chains can be indeed stabilized through the association of K63-linkage-specific ubiquitin-binding proteins that protect them from proteasomal degradation (40, 41). Alternatively, although not yet determined, the formation of K63-linked chains on JARID1B might act in a completive manner toward the attachment of K48-polyubiquitin chains by another E3, exerting instead a proteolytic role. Regulation of JARID1B degradation is still a quite unexplored field, with the S-phase kinase-associated protein-2 (SKP2), a component of the E3 SCF complex, being one of the very few E3 responsible for its proteolysis (42). However, the Lys residue targeted by SKP2 in JARID1B (43) seems to differ from that modified by WWP1, ruling out its contribution in this context. Further studies are

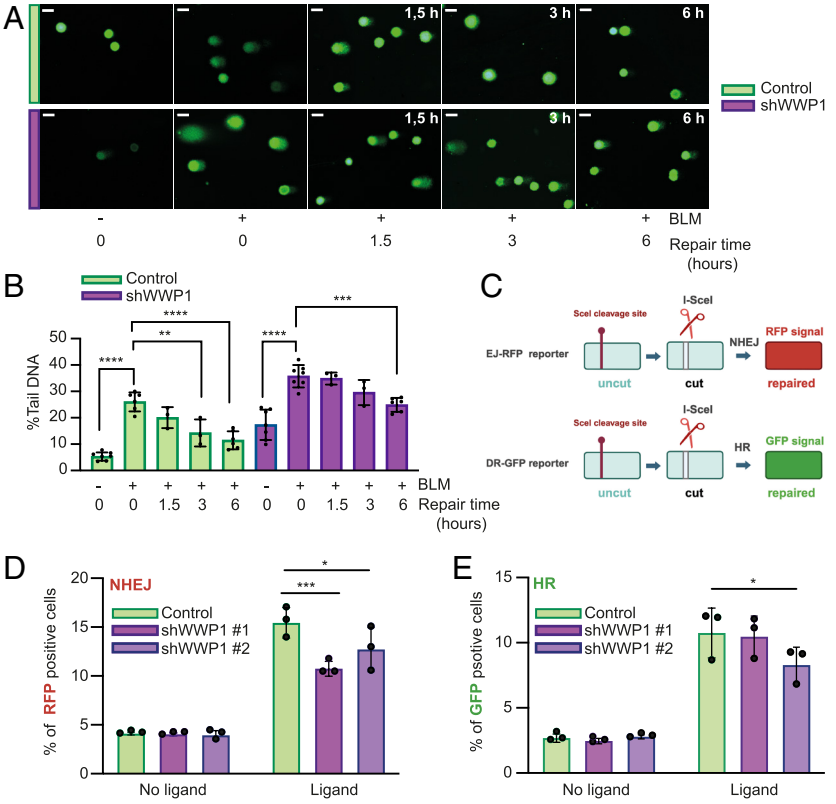

Fig. 6. DNA damage resolution is delayed in WWP1-depleted cells. (*A* and *B*) DNA damage and repair activity were assessed by a comet-based assay performed at different time points following BLM washout. Representative fluorescence images. (Scale bar, 50 μm.) (*A*) and quantification (*B*) in percentage of tail DNA. The parameter % tail DNA was measured with ImageJ from 100 randomly selected cells for each condition. Three independent experiments were carried out. Values represent the mean ± SD from three or six independent experiments. Statistical significance was calculated using the one-way ANOVA test. $^{**}P < 0.01$, $^{***}P < 0.001$, $^{****}P < 0.0001$. (*C*) Schematic representation of the EJ-RFP and DR-GFP reporter assays. The U2OS EJ-DRs cell line (38) contains integrated copies of both assays. NHEJ activity can be detected as an increase in RFP^+ cells, while HR activation is measured as in increase in GFP^+ cells. (*D* and *E*) The percentages of RFP^+ and GFP^+ cells reflect the levels of NHEJ and HR activation, respectively. Values represent the mean ± SD from three independent experiments. Statistically significant differences were calculated by the two-way ANOVA *t* test. $^{*}P < 0.05$, $^{***}P < 0.001$.

needed to shed light on the molecular determinants of JARID1B stabilization by WWP1.

Destabilization of JARID1B resulting from WWP1 inactivation impairs its histone demethylase activity, as revealed by enhanced global levels of H3K4me3, increased enrichment of H3K4me3 peaks at JARID1B target genes, with subsequent reactivation of their expression. Remarkably, one of the most up-regulated JARID1B target genes in WWP1-depleted cells is the cell cycle

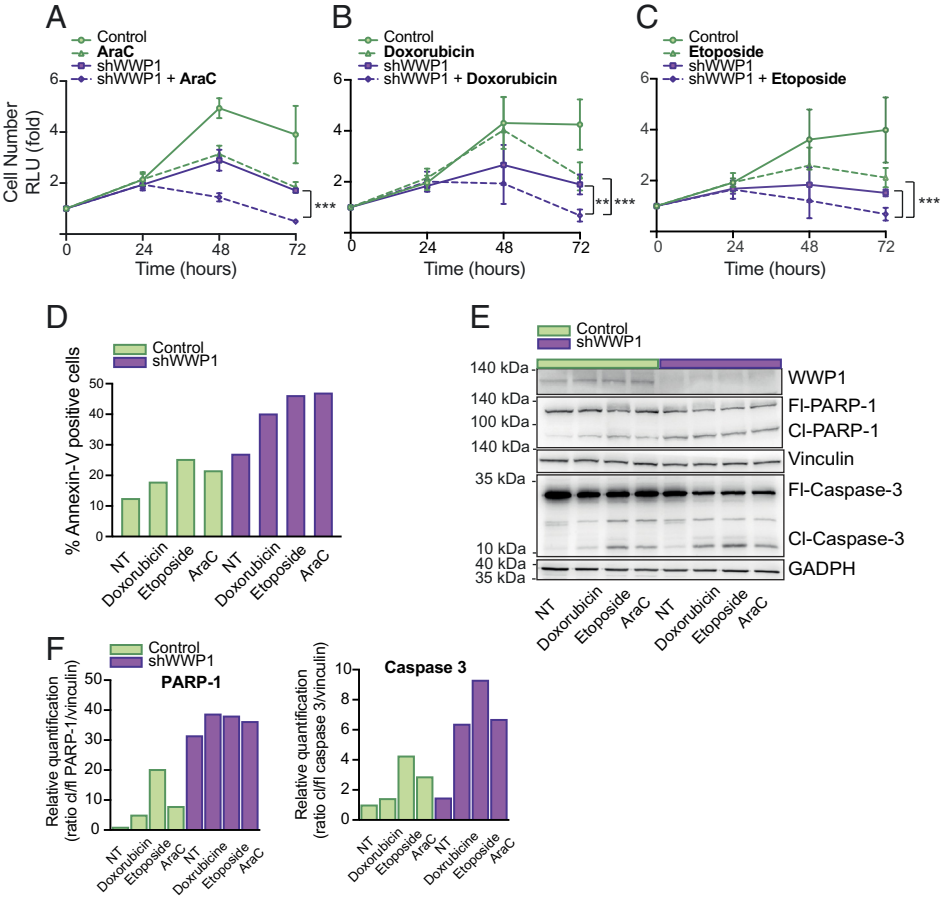

Fig. 7. WWP1 silencing sensitizes AML cells to DNA-damaging chemotherapeutic drugs. Control and WWP1-depleted cells were exposed to AraC (*A*), doxorubicin (*B*), and etoposide (*C*), and cell viability was assessed by the CellTiter-Glo® assay. Values represent the mean ± SD from three independent experiments. Statistically significant differences were calculated by Student's *t* test. $^{**}P < 0.01$, $^{***}P < 0.001$. (*D–F*) Evaluation of apoptosis in control and WWP1-depleted NB4 cells exposed to chemotherapy. (*D*) Representative percentages of apoptotic cells, assessed by flow cytometry after staining with FITC annexin-V conjugates and DAPI. Three independent experiments were carried out. (*E*) Representative western blot analysis of cleaved PARP1 and caspase-3 proteins. (*F*) Densitometric quantification of cleaved (cl)/full-length (fl) ratio for PARP (*Left* panel) and caspase 3 (*Right* panel), respectively. Three independent experiments were carried out.

inhibitor *CDKN1A*/p21. This evidence strongly supports the relevance of the WWP1/JARID1B functional axis in leukemia. Both WWP1 silencing and JARID1B inhibition indeed promote cell cycle arrest of leukemic cells (18, 19), implying that deregulation of WWP1 might be responsible for sustaining the repression of *CDKN1A*/p21 expression through the ubiquitin-dependent activation of JARID1B.

Chromatin is dynamically remodeled to adapt DDR. Epigenetic regulation of chromatin structure indeed contributes to efficient DNA damage response signaling through several different mechanisms. First, histone modifications such as H2AX phosphorylation, H2A ubiquitination at K13/15, and H4K20me2 create a signal for recruitment of the DSB repair proteins (3). Another layer of the regulatory mechanism invoked upon DNA damage is accomplished by chromatin remodeling complexes and histone modifiers that act on chromatin architecture to elicit its decondensation (44). Additionally, regulation of some histone modifications such as demethylation of H3K4me3 by JARID1B creates a permissive chromatin structure for the recruitment of repair factors in response to DNA damage (22–24). Similarly to JARID1B inhibition, and concomitantly with increased H3K4me3 levels, we observed an overall defective recruitment of DDR factors upon DNA damage induction in WWP1-depleted AML cells (Fig. 8). Coherently, the efficiency of DNA repair was hampered upon WWP1 inactivation, with no obvious preference for a specific DNA repair signaling pathway. The formation of DDR foci following BLM administration was indeed impaired in WWP1-silenced leukemia cells for components of both the DNA DSBs repair systems: NHEJ and HR. Evaluation of DNA DSB break repair capacity by employing reporter assays also confirmed that both systems were affected by knocking down WWP1, although at different extent.

Defective repair capacity in WWP1-depleted cells was associated with increased sensitivity of leukemic blasts to DNA-damaging chemotherapeutic agents (Fig. 8). The role of WWP1 in the response of tumor cells to anticancer therapies is poorly explored and the molecular basis for WWP1's ability to influence the efficacy of chemotherapy remains unknown. WWP1 inhibition via the natural compound indole-3-carbinol has been shown to enhance the efficacy of PI3K inhibitors to suppress breast cancer tumor growth (45). A contribution of WWP1 to the responsiveness of cancer cells to genotoxic drugs has been reported by Li and colleagues, who demonstrated that WWP1 knockdown increases the sensitivity of colon cancer cells to doxorubicin and cisplatin via a p63-dependent mechanism (46). Since p53 is a target of WWP1 (47), it could likely be a general mediator of its ability to modulate chemosensitivity. However, the cellular model employed in this study carries mutant p53, thus ruling out any involvement of p53 in WWP1-mediated regulation of DNA damage repair. While we cannot exclude the existence of additional yet unknown WWP1 substrates implicated in the DDR and of concomitant regulatory mechanisms underlying the contribution of WWP1 to DNA damage repair, our findings establish the existence of a WWP1/JARID1B functional axis sustaining AML chemoresistance.

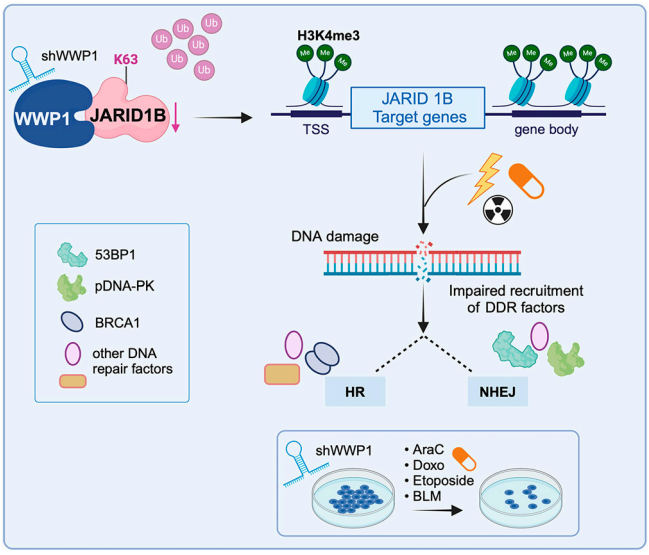

Fig. 8. A model depicting the outcome of WWP1 silencing in AML cells. WWP1 inactivation reduces JARID1B ubiquitination and, in turn, decreases its cellular availability, enhancing the global levels of H3K4 trimethylation in chromatin. This change in chromatin composition would then hinder the recruitment of DNA repair factors and DNA repair efficiency, leading to accumulation of DNA damage and increased toxicity elicited by genotoxic drugs.

Materials and Methods

UbiScan®. Samples were analyzed using the PTMScan method provided by Cell Signaling Technology as previously described (25, 48). Total protein extracts were digested with trypsin and enriched with the Ubiquitin K-GG Remnant Motif antibody. MS/MS spectra were evaluated using SEQUEST (49) and the Core platform from Harvard University. Significant hits were defined with a 2.5-fold cut-off between compared samples, a minimum peptide intensity of 200,000, and a maximum percent coefficient of variation of 50%.

Cell Culture and Treatments. The tetracycline (Tet)-On-inducible NB4 cells (NB4/Tet-On/shWWP1 cells) (8) were cultured in RPMI medium supplemented with 10% tetracycline-free (Tet-free) FBS and Pen/Strept. U2OS EJ-DR cells (a kind gift of Dr Simon Powell, Memorial Sloan Kettering Cancer Center, NY) were cultured in high-glucose DMEM with l-glutamine containing 10% Tet-free FBS and Pen/Strep, as previously described (38).

Cloning and Cell Transfection. Transfection was performed with Lipofectamine 3000 (Invitrogen) or Effectene (Qiagen). Mutagenesis was performed using the In-Fusion Cloning kit (Takara), according to the manufacturer's instructions. Sequences of primers employed for mutagenesis are listed in *SI Appendix*, Table S1.

Protein Extraction and Western Blot Analysis. Protein lysates in Triton-X-100 buffer with protease and phosphatase inhibitors were resolved on SDS-PAGE gels and transferred to polyvinylidene fluoride (PVDF) membranes. Membranes were blocked in 5% nonfat dry milk/BSA, incubated overnight with primary antibodies, washed in PBS-Tween 0,1%, incubated with secondary antibodies, developed using SuperSignal ECL, and then scanned at the UVITEC. Primary and secondary antibodies are listed in *SI Appendix, Materials and Methods*.

Immunoprecipitation Experiments. After a precleaning step of 4 to 6 h at 4 °C in rotation with Protein A sepharose beads (4 Fast flow, Cytiva 17528001), 1 to 5 mg total protein extracts were incubated with specific antibody-conjugated affinity beads. After washing, protein elution was performed by boiling the samples in loading buffer and centrifugation, prior to electrophoresis.

In Vitro Pull-Down Assays. Recombinant proteins (300 ng; Abcam) were incubated overnight at 4 °C in binding buffer (50mM Tris-HCl, pH7.5, 150mM NaCl, 0.1% Nonidet NP-40, and 1mM EDTA). On the same time, anti-WWP1 antibody (Novus NBP1-49713) was incubated with Protein A beads. Afterward, proteins were incubated with the antibody–beads complexes left 3 h at 4 °C. Finally, the samples were boiled in loading buffer and then used for gel electrophoresis.

In Vitro Ubiquitination Assay. Recombinant JARID1B (50 ng) and WWP1 (40 ng) proteins were incubated in 50 mM Tris-HCl, pH 7.5, 5mM MgCl2 buffer, with 6 mM ATP, 0,6 mM DTT, 40 ng UbcH5 E2 (R&D System), 50 ng UBE1 (R&D System), and 1 μg wild-type or K-R ubiquitin mutants (UBPBio) Samples were left for 2 h at 30 °C and then incubated at 98 °C for 5 min with loading buffer prior to gel electrophoresis.

RNA Extraction, cDNA Synthesis, and RT-qPCR. The RNeasy mini kit (Qiagen; catalog 74004) was used for RNA isolation. RNA concentration was measured with a NanoDrop Spectrophotometer (Thermo Scientific). RNA was reverse transcribed with the SensiFAST cDNA Synthesis Kit (Bioline; catalog BIO-65053). Real Time-qPCR was performed in a Q5 Real-Time PCR System (Applied Biosystems) using SensiFAST™ Probe Lo-ROX Kit (Meridian Bioscience, BIO-84050). Primer sequences are listed in Dataset S6.

ChIP Sequencing. ChIP-seq for the histone mark H3K4me3 was performed by Active Motif (Carlsbad, CA). Experimental and analysis details are included in *SI Appendix, Materials and Methods*.

RNA Sequencing. The RNA sequencing (RNA-Seq) analysis was conducted using the "mRNA Stranded TruSeq" library preparation protocol. Sequencing was performed on the NovaSeq 6000 platform using the S2 flow cell. Raw sequencing data were processed using standard bioinformatics tools as detailed in *SI Appendix, Materials and Methods*. To test for the overlap of overexpressed genes in RNAseq with potential KDM5B target genes we used the "Target Genes" prediction by the ChIP-Atlas (50) (https://chip-atlas.org/target_genes) using 1kb as distance from the TSS. We then downloaded JARID1B putative target genes showing binding scores ≥ 500 from the SRX186782 (SRA, short read archive) dataset in ENCODE (https://chip-atlas.dbcls.jp/data/hg38/target/KDM5B.1.html) Overlap Venn and Fisher statistics were calculated with the 'Compare Set Appyters' (51). Functional enrichment was performed using Enrichr (52) and pathways were considered significant when showing an FDR < 0.05

Clinical Samples. Leukemic samples were obtained from bone marrow aspirates of patients diagnosed with de novo AML at the Hematology Unit of the Department of Biomedicine and Prevention of the University of Tor Vergata. Informed consent was obtained from all patients according to the Declaration of Helsinki and the study was approved by the Institutional Review Board of "Policlinico Tor Vergata Hospital." All human participants gave written informed consent.

Immunofluorescence of DDR foci. Cells were fixed with paraformaldehyde, washed, and then permeabilized with 0.1% Triton. Blocking was performed in 5% goat serum for 1 h prior to overnight incubation with primary antibodies (detailed in *SI Appendix, Materials and Methods*), followed by incubation with secondary antibodies and DAPI. Images were acquired at a confocal microscope (Stellaris 5, Leica).

Comet Assay. Cells were resuspended in low melting agarose and spread on Comet slides (Trevigen). The slides were immersed in Lysis Solution (Comet assay Trevigen kit) at 4 °C overnight. After incubation in prechilled alkaline unwinding solution, electrophoresis was performed. The slides were then immersed in 70% EtOH and dried. DNA staining was stained with SYBR Green.

EJ-DR Reporter System. NHEJ and HR repair activities were measured as previously described (37). Experimental details can be found in *SI Appendix, Materials and Methods*.

Apoptotic Assays. Cells were incubated with FITC-conjugated Annexin V and DAPI according to the manufacturer's instructions (Becton Dickinson). Stained cells were analyzed using the CytoFLEX cytometer.

Bioinformatic Analyses. The TCGA AML gene expression values were retrieved using Xena Browser (https://xenabrowser.net/). The differential expression analysis was performed using DESeq2 package from Xena Browser. Values were represented as volcano plot using ggplot2 package. Correlation between *CDKN1A* and *WWP1* expression levels was visualized using ggpointdensity and viridis packages.

Statistical Analysis. Results were shown as mean ± SD or SEM, and statistical significance was calculated by ANOVA, Kruskal–Wallis test, or Student's t test as specified in the figure legends. Violin plots were generated using ggplot2 package.

Data, Materials, and Software Availability. All study data are included in the article and/or *SI Appendix*.

ACKNOWLEDGMENTS. We gratefully acknowledge Dr Simon Powell (Memorial Sloan Kettering Cancer Center, NY) for sharing the EJ-DR U2OS reporter cell line. The Research leading to these results has received funding from AIRC under IG 2019–23232–P.I. Bernassola Francesca. This work has been also supported by the MUR-PNRR M4C2I1.3 PE6 project PE00000019 Heal Italia (CUP: E83C22004670001) to G.M., E.C., and F.B. and Fondazione Luigi Maria Monti IDI-IRCCS (R.C. to E.C.).

Author affiliations: [a]Department of Experimental Medicine, Tor Vergata Oncoscience Research, University of Rome Tor Vergata, Rome 00133, Italy; [b]Biochemistry Laboratory, Istituto Dermopatico Immacolata, Rome 00100, Italy; [c]The First Affiliated Hospital of Soochow University, Institutes for Translational Medicine, Soochow University, Suzhou 215000, China; [d]Institutes of Biology and Medical Sciences, Suzhou Medical College, Soochow University, Suzhou, Jiangsu 215000, China; [e]Center for Omics Sciences, Istituti di Ricovero e Cura a Carattere Scientifico, San Raffaele Scientific Institute, Milan 20132, Italy; [f]Lymphoid stromal cell biology Unit, Division of Experimental Oncology, Istituti di Ricovero e Cura a Carattere Scientifico, San Raffaele Scientific Institute, Milan 20132, Italy; and [g]Systems Toxicology, Department of Biology, University of Konstanz, Konstanz 78464, Germany

1. N. J. Short, M. E. Rytting, J. E. Cortes, Acute myeloid leukaemia. *Lancet* **392**, 593–606 (2018).
2. P. Karakaidos, D. Karagiannis, T. Rampias, Resolving DNA damage: Epigenetic regulation of DNA repair. *Molecules* **25**, 2496 (2020).
3. S. Min, J.-H. Ji, Y. Heo, H. Cho, Transcriptional regulation and chromatin dynamics at DNA double-strand breaks. *Exp. Mol. Med.* **54**, 1705–1712 (2022).
4. S. P. Jackson, J. Bartek, The DNA-damage response in human biology and disease. *Nature* **461**, 1071–1078 (2009).
5. A. G. Sanarico *et al.*, The E3 ubiquitin ligase WWP1 sustains the growth of acute myeloid leukaemia. *Leukemia* **32**, 911–919 (2018).
6. V. S. Delvecchio, C. Fierro, S. Giovannini, G. Melino, F. Bernassola, Emerging roles of the HECT-type E3 ubiquitin ligases in hematological malignancies. *Discov. Oncol.* **12**, 39 (2021).
7. F. Bernassola, G. Chillemi, G. Melino, Hect-type E3 ubiquitin ligases in cancer. *Trends Biochem. Sci.* **44**, 1057–1075 (2019).
8. S. Giovannini *et al.*, Thioredoxin-interacting protein (TXNIP) is a substrate of the NEDD4-like E3 ubiquitin-protein ligase WWP1 in cellular redox state regulation of acute myeloid leukemia cells. *Mol. Oncol.* **19**, 133–150 (2024).
9. M. T. Pedersen, K. Helin, Histone demethylases in development and disease. *Trends Cell Biol.* **20**, 662–671 (2010).
10. L. Xie *et al.*, KDM5B regulates embryonic stem cell self-renewal and represses cryptic intragenic transcription. *EMBO J.* **30**, 1473–1484 (2011).
11. Y. Xiang *et al.*, JARID1B is a histone H3 lysine 4 demethylase up-regulated in prostate cancer. *Proc. Natl. Acad. Sci. U.S.A.* **104**, 19226–19231 (2007).
12. Z. Wang *et al.*, KDM5B is overexpressed in gastric cancer and is required for gastric cancer cell proliferation and metastasis. *Am. J. Cancer Res.* **5**, 87–100 (2015).
13. B. R. Leadem *et al.*, A KDM5 inhibitor increases global H3K4 trimethylation occupancy and enhances the biological efficacy of 5-aza-2′-deoxycytidine. *Cancer Res.* **78**, 1127–1139 (2018).
14. B. Zhang *et al.*, Deubiquitinase USP7 stabilizes KDM5B and promotes tumor progression and cisplatin resistance in nasopharyngeal carcinoma through the ZBTB16/TOP2A axis. *Cell Death Differ.* **31**, 309–321 (2024).
15. S. Scalea *et al.*, Modifications of H3K4 methylation levels are associated with DNA hypermethylation in acute myeloid leukemia. *FEBS J.* **287**, 1155–1175 (2020).
16. Z. Ren *et al.*, A PRC2-Kdm5b axis sustains tumorigenicity of acute myeloid leukemia. *Proc. Natl. Acad. Sci. U.S.A.* **119**, e2122940119 (2022).
17. S. H. K. Wong *et al.*, The H3K4-methyl epigenome regulates leukemia stem cell oncogenic potential. *Cancer Cell* **28**, 198–209 (2015).
18. G. Shokri, S. Doudi, M. Fathi-Roudsari, F. Kouhkan, M.-H. Sanati, Targeting histone demethylases KDM5A and KDM5B in AML cancer cells: A comparative view. *Leuk. Res.* **68**, 105–111 (2018).
19. Y.-Q. Huang, Y. Zou, R.-J. Zheng, X.-D. Ma, Down-regulation of JARID1B expression inhibits cell proliferation, induces apoptosis and blocks cell cycle in human acute lymphoblastic leukemia cells. *Eur. Rev. Med. Pharmacol. Sci.* **22**, 1366–1373 (2018).
20. P.-P. Wong *et al.*, Histone demethylase KDM5B collaborates with TFAP2C and Myc to repress the cell cycle inhibitor p21(cip) (CDKN1A). *Mol. Cell Biol.* **32**, 1633–1644 (2012).
21. D. Wang *et al.*, Depletion of histone demethylase KDM5B inhibits cell proliferation of hepatocellular carcinoma by regulation of cell cycle checkpoint proteins p15 and p27. *J. Exp. Clin. Cancer Res.* **35**, 37 (2016).
22. J. Bayo *et al.*, Jumonji inhibitors overcome radioresistance in cancer through changes in H3K4 methylation at double-strand breaks. *Cell Rep.* **25**, 1040–1050.e5 (2018).
23. X. Li *et al.*, Histone demethylase KDM5B is a key regulator of genome stability. *Proc. Natl. Acad. Sci. U.S.A.* **111**, 7096–101 (2014).
24. W. Xu *et al.*, KDM5B demethylates H3K4 to recruit XRCC1 and promote chemoresistance. *Int. J. Biol. Sci.* **14**, 1122–1132 (2018).
25. M. P. Stokes *et al.*, Complementary PTM profiling of drug response in human gastric carcinoma by immunoaffinity and IMAC methods with total proteome analysis. *Proteomes* **3**, 160–183 (2015).
26. L. Rheinemann *et al.*, Interactions between AMOT PPxY motifs and NEDD4L WW domains function in HIV-1 release. *J. Biol. Chem.* **297**, 100975 (2021).
27. A. Peschiaroli, F. Scialpi, F. Bernassola, E. S. El Sherbini, G. Melino, The E3 ubiquitin ligase WWP1 regulates ΔNp63-dependent transcription through Lys63 linkages. *Biochem. Biophys. Res. Commun.* **402**, 425–430 (2010).
28. M. E. French *et al.*, Mechanism of ubiquitin chain synthesis employed by a HECT domain ubiquitin ligase. *J. Biol. Chem.* **292**, 10398–10413 (2017).
29. Y.-R. Lee *et al.*, Reactivation of *PTEN* tumor suppressor for cancer treatment through inhibition of a *MYC-WWP1* inhibitory pathway. *Science* **364**, eaau0159 (2019).

30. A. Janzer *et al.*, The H3K4me3 histone demethylase Fbxl10 is a regulator of chemokine expression, cellular morphology, and the metabolome of fibroblasts. *J. Biol. Chem.* **287**, 30984–30992 (2012).
31. D. Komander, M. Rape, The ubiquitin code. *Annu. Rev. Biochem.* **81**, 203–229 (2012).
32. Z. J. Chen, L. J. Sun, Nonproteolytic functions of ubiquitin in cell signaling. *Mol. Cell* **33**, 275–286 (2009).
33. S. U. Schmitz *et al.*, Jarid1b targets genes regulating development and is involved in neural differentiation. *EMBO J.* **30**, 4586–4600 (2011).
34. T. T. Paull *et al.*, A critical role for histone H2AX in recruitment of repair factors to nuclear foci after DNA damage. *Curr. Biol.* **10**, 886–895 (2000).
35. I. M. Ward, K. Minn, K. G. Jorda, J. Chen, Accumulation of checkpoint protein 53BP1 at DNA breaks involves its binding to phosphorylated histone H2AX. *J. Biol. Chem.* **278**, 19579–82 (2003).
36. T. Lei, S. Du, Z. Peng, L. Chen, Multifaceted regulation and functions of 53BP1 in NHEJ-mediated DSB repair (Review). *Int. J. Mol. Med.* **50**, 90 (2022).
37. T. A. Dobbs, J. A. Tainer, S. P. Lees-Miller, A structural model for regulation of NHEJ by DNA-PKcs autophosphorylation. *DNA Repair (Amst.)* **9**, 1307–1314 (2010).
38. R. S. Bindra, A. G. Goglia, M. Jasin, S. N. Powell, Development of an assay to measure mutagenic non-homologous end-joining repair activity in mammalian cells. *Nucleic Acids Res.* **41**, e115 (2013).
39. M. R. Litzow, Progress and strategies for patients with relapsed and refractory acute myeloid leukemia. *Curr. Opin. Hematol.* **14**, 130–137 (2007).
40. J. A. Nathan, H. T. Kim, L. Ting, S. P. Gygi, A. L. Goldberg, Why do cellular proteins linked to K63-polyubiquitin chains not associate with proteasomes? *EMBO J.* **32**, 552–565 (2013).
41. M. Liu *et al.*, Macrophage K63-linked ubiquitination of YAP promotes its nuclear localization and exacerbates atherosclerosis. *Cell Rep.* **32**, 107990 (2020).
42. Y. Liu, Y. Zhou, Circ_0087960 stabilizes KDM5B by reducing SKP2 mediated ubiquitination degradation and promotes osteogenic differentiation in periodontal ligament stem cells. *Regener. Ther.* **19**, 122–130 (2022).
43. W. Lu *et al.*, SKP2 inactivation suppresses prostate tumorigenesis by mediating JARID1B ubiquitination. *Oncotarget* **6**, 771–788 (2015).
44. J. Dabin, A. Fortuny, S. E. Polo, Epigenome maintenance in response to DNA damage. *Mol. Cell* **62**, 712–727 (2016).
45. T. Kishikawa *et al.*, *WWP1* inactivation enhances efficacy of *PI3K* inhibitors while suppressing their toxicities in breast cancer models. *J. Clin. Invest.* **131**, e140436 (2021).
46. Y. Li, Z. Zhou, C. Chen, WW domain-containing E3 ubiquitin protein ligase 1 targets p63 transcription factor for ubiquitin-mediated proteasomal degradation and regulates apoptosis. *Cell Death Differ.* **15**, 1941–1951 (2008).
47. A. Laine, Z. Ronai, Regulation of p53 localization and transcription by the HECT domain E3 ligase WWP1. *Oncogene* **26**, 1477–1483 (2007).
48. V. J. Gennaro *et al.*, Control of CCND1 ubiquitylation by the catalytic SAGA subunit USP22 is essential for cell cycle progression through G1 in cancer cells. *Proc. Natl. Acad. Sci. U.S.A.* **115**, E9298–E9307 (2018).
49. J. K. Eng, A. L. McCormack, J. R. Yates, An approach to correlate tandem mass spectral data of peptides with amino acid sequences in a protein database. *J. Am. Soc. Mass Spectrom.* **5**, 976–989 (1994).
50. Z. Zou, T. Ohta, S. Oki, CHIP-atlas 3.0: A data-mining suite to explore chromosome architecture together with large-scale regulome data. *Nucleic Acids Res.* **52**, W45–W53 (2024).
51. D. J. B. Clarke *et al.*, Appyters: Turning Jupyter notebooks into data-driven web apps *Patterns* **2**, 100213 (2021).
52. Z. Xie *et al.*, Gene set knowledge discovery with Enrichr. *Curr. Protoc.* **1**, e90 (2021).